平成26年度厚生労働科学研究費補助金（H26-化学-一般-001）

吸入暴露影響の情動認知行動解析と神経科学的物証の収集

研究分担者　種村健太郎

東北大学大学院農学研究科　動物生殖科学分野・教授

1

研究の背景

吸入毒性試験において病理組織学的な病変を誘発する暴露濃度は、人のシックハウス症候群（SHS）の指針濃度をはるかに超える濃度であることから、毒性試験から得た情報を人へ外挿することの困難さが指摘されており、特に異常行動への関与の有無を含めた中枢神経系への影響については、神経科学的な物証を伴わない、心理学的な記載による報告が多かった。

2

研究目的

そこで、本分担研究では、反復暴露の結果の検証とその判定根拠の一般化を目指し、SHSレベル暴露実験を実施し、情動認知行動解析と神経科学的物証の収集による海馬に対する有害性の実証、及び遺伝子発現変動データの予見性の確認、を目的とする。
尚、この際、脳が高感受性期に当たる可能性から子どもの特性に配慮した遅発性影響も検討する。

3

方法

異常行動への関与の有無を含めた中枢神経系への影響を検討する目的で行う情動認知行動解析において、可能な限り混交要因を排除するため、様々な取り組みが行われているが、解析装置まで動物を輸送する際に、動物に与えるストレスが高精度解析を妨げる恐れが指摘されている。
そこで我々は吸入暴露装置に出来るだけ近い場所に行動解析機器を用意することで、上記の混交要因の排除を試みた。

移動可能な架台式行動解析バッテリーユニット
移動可能な車輪をつけた防音箱内でオープンフィールド試験、明暗往来試験、条件付け学習記憶試験を行うことができる。

4

方法

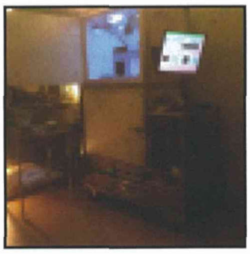

オープンフィールド試験: OF

明暗往来試験: LD

条件付け学習記憶試験: FZ

移動可能な架台式行動解析バッテリーユニット

移動可能な車輪をつけた防音箱内でオープンフィールド試験、明暗往来試験、条件付け学習記憶試験を行うことができる。

5

吸入暴露および情動認知行動解析室の内観

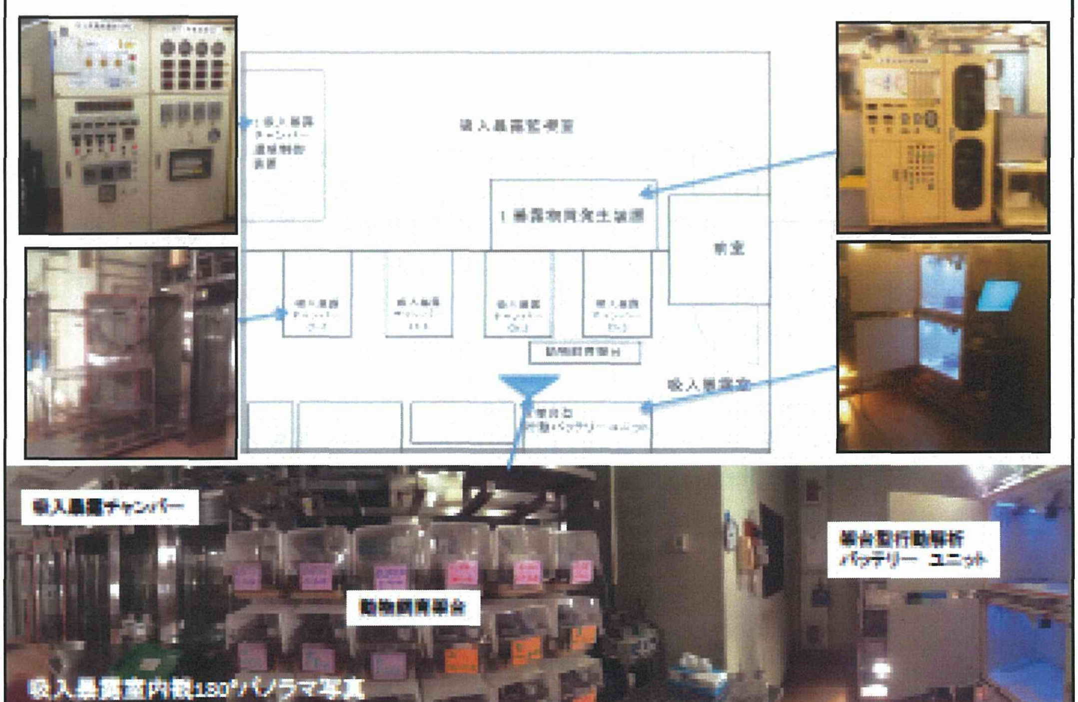

結果

移動式行動解析装置によるマウス行動解析は、従来の結果を再現可能であり、本研究遂行に支障がないことが確認された。

成熟期マウスへのキシレン吸入暴露による情動認知行動影響の解析

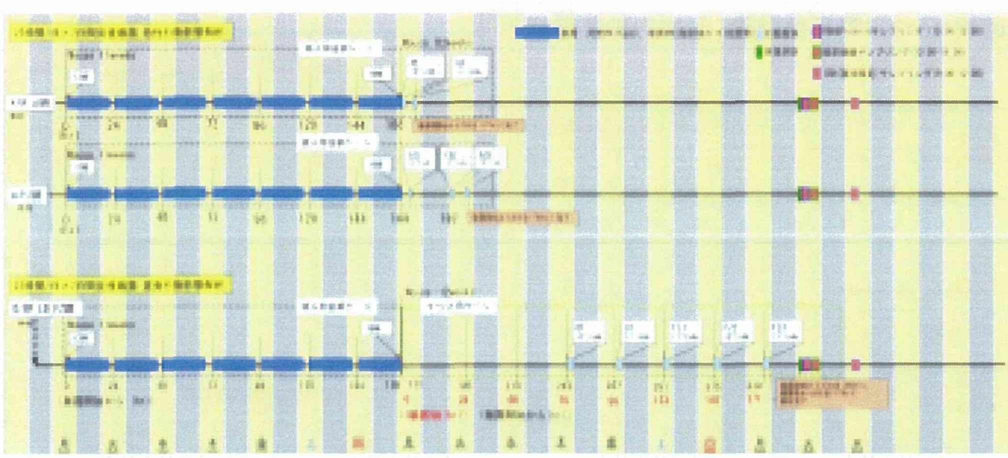

照明周期

PM8:00	AM8:00 (約60lux)

略号		試験名	測定項目	試験に要する時間
OF		Open field test	新奇環境・活動性	N=8, 2群(16匹)で120分
LD		Light / Dark transition test	不安関連行動	N=8, 2群(16匹)で50分
FZ	FZ1	Fear conditioning: Conditioning	トレーニング／短期学習	N=8, 2群(16匹)で70分
	FZ2	Fear conditioning: Contextual test	空間記憶	N=8, 2群(16匹)で70分
	FZ3	Fear conditioning: Cued test	音・連想記憶	N=8, 2群(16匹)で70分

情動-認知行動解析

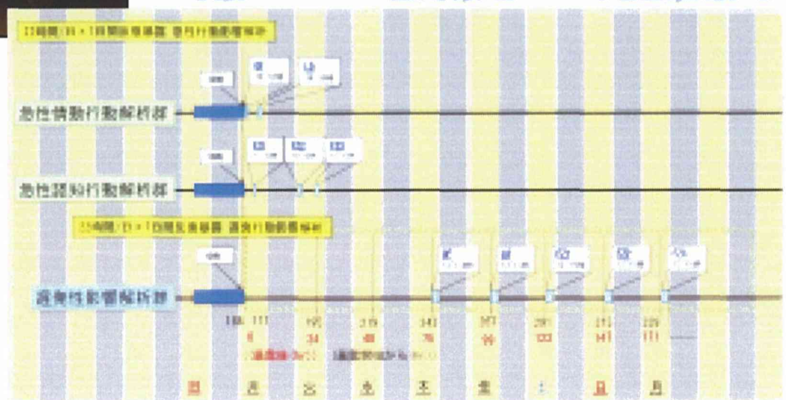

成熟期マウスへのキシレン吸入暴露による情動認知行動影響の解析

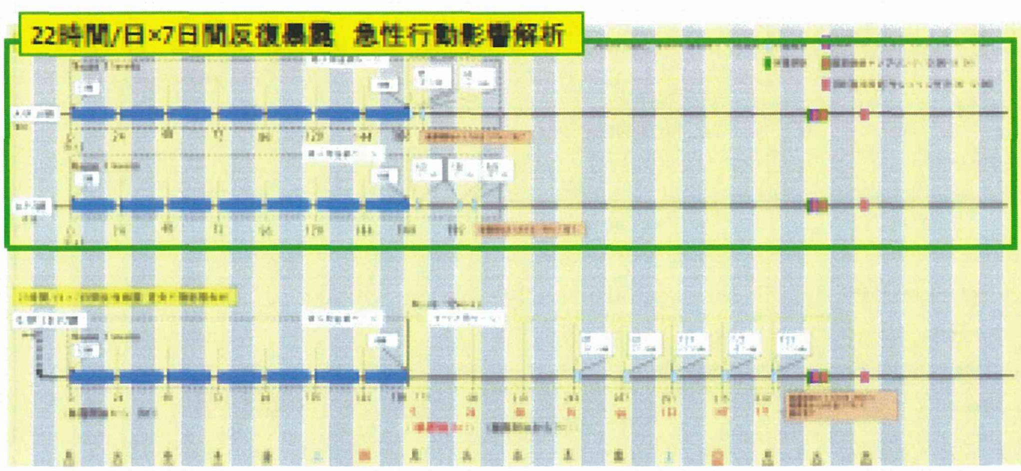

照明周期

PM8:00　AM8:00 (約60lux)

略号	試験名	測定項目	試験に要する時間
OF	Open field test	新奇環境・活動性	N=8, 2群(16匹)で120分
LD	Light / Dark transition test	不安関連行動	N=8, 2群(16匹)で90分
FZ FZ1	Fear conditioning: Conditioning	トレーニング/短期学習	N=8, 2群(16匹)で70分
FZ FZ2	Fear conditioning: Contextual test	空間記憶	N=8, 2群(16匹)で70分
FZ FZ3	Fear conditioning: Cued test	音-連想記憶	N=8, 2群(16匹)で70分

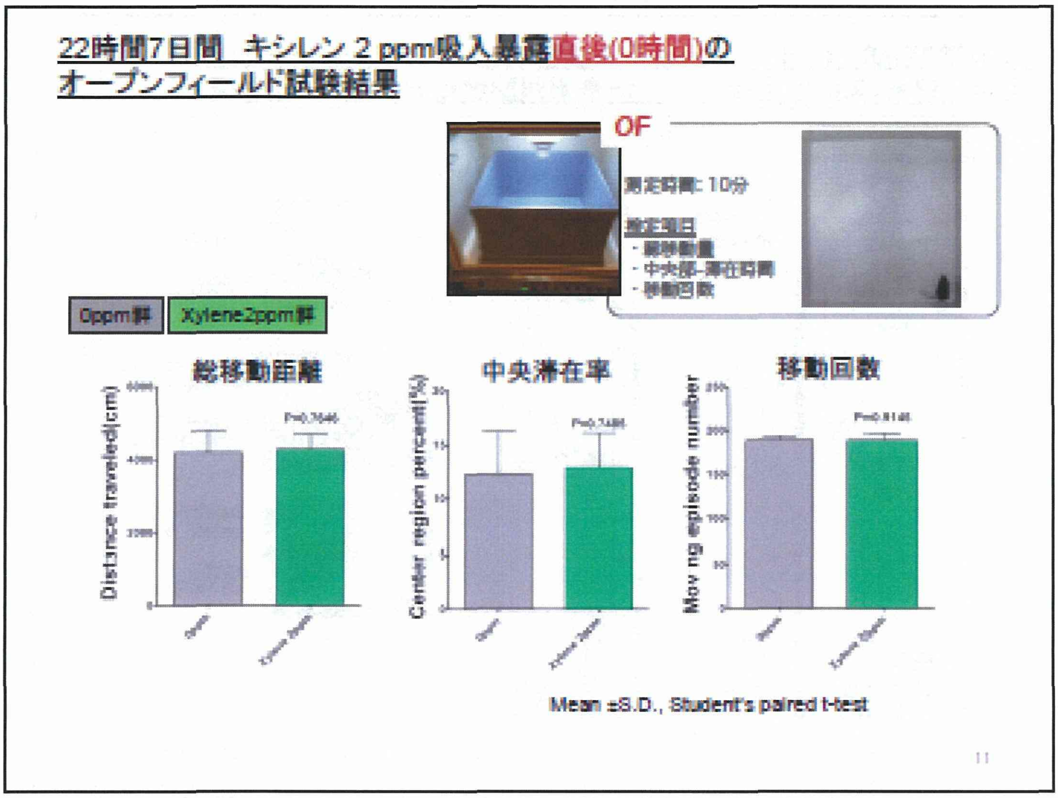
22時間7日間 キシレン 2 ppm吸入暴露直後(0時間)の
オープンフィールド試験結果
OF
測定時間: 10分
測定項目
0ppm群
Xylene2ppm群
総移動距離
中央滞在率
移動回数
Distance traveled(cm)
Center region percent(%)
Mov ng episode number
Mean ±S.D., Student's paired t-test
11

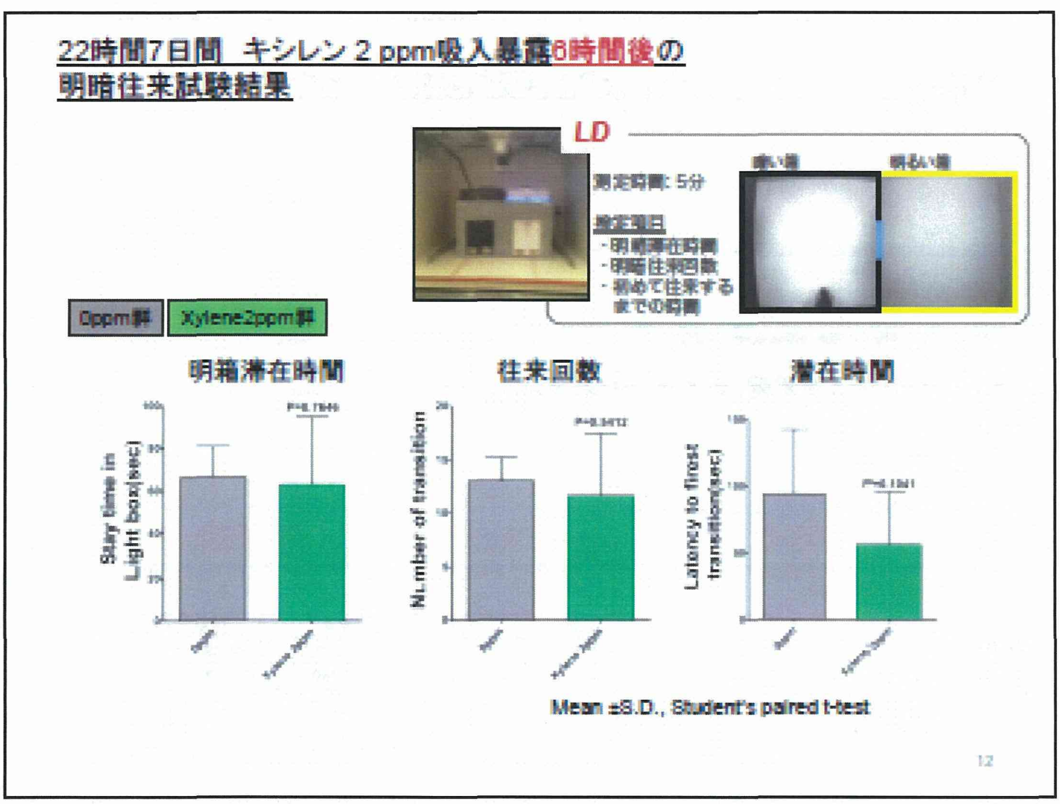
22時間7日間 キシレン 2 ppm吸入暴露6時間後の
明暗往来試験結果
LD
測定時間: 5分
測定項目
・明暗滞在時間
・明暗往来回数
・初めて往来する
までの時間
0ppm群
Xylene2ppm群
明箱滞在時間
往来回数
潜在時間
Stay time in Light box(sec)
Number of transition
Latency to first transition(sec)
Mean ±S.D., Student's paired t-test
12

22時間7日間 キシレン 2 ppm吸入暴露3時間後に条件付け(FZ1)、翌日に場所-連想記憶試験(FZ2)と音連想記憶試験(FZ3)をした結果

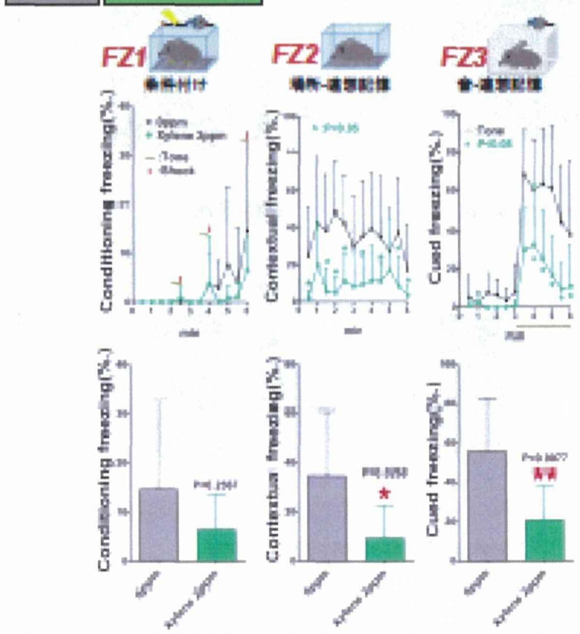

13

成熟期マウスへのキシレン吸入暴露による情動認知行動影響の解析

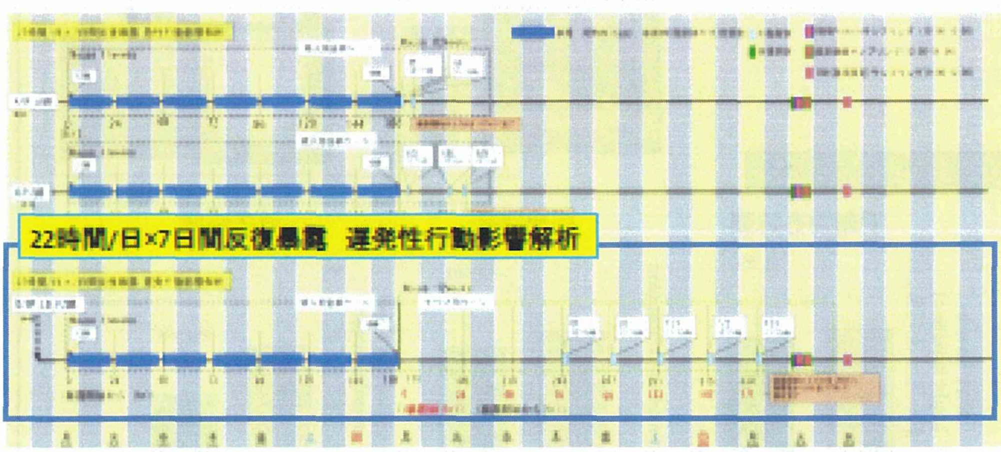

明暗周期

PM8:00 | AM8:00 (約60lux)

略号		試験名	測定項目	試験に要する時間
OF		Open field test	新奇環境・活動性	N=6, 3群(18匹)で120分
LD		Light / Dark transition test	不安関連行動	N=6, 3群(18匹)で60分
FZ	FZ1	Fear conditioning: Conditioning	トレーニング/短期学習	N=6, 3群(18匹)で70分
	FZ2	Fear conditioning: Contextual test	空間記憶	N=6, 3群(18匹)で70分
	FZ3	Fear conditioning: Cued test	音ー連想記憶	N=6, 3群(18匹)で70分

14

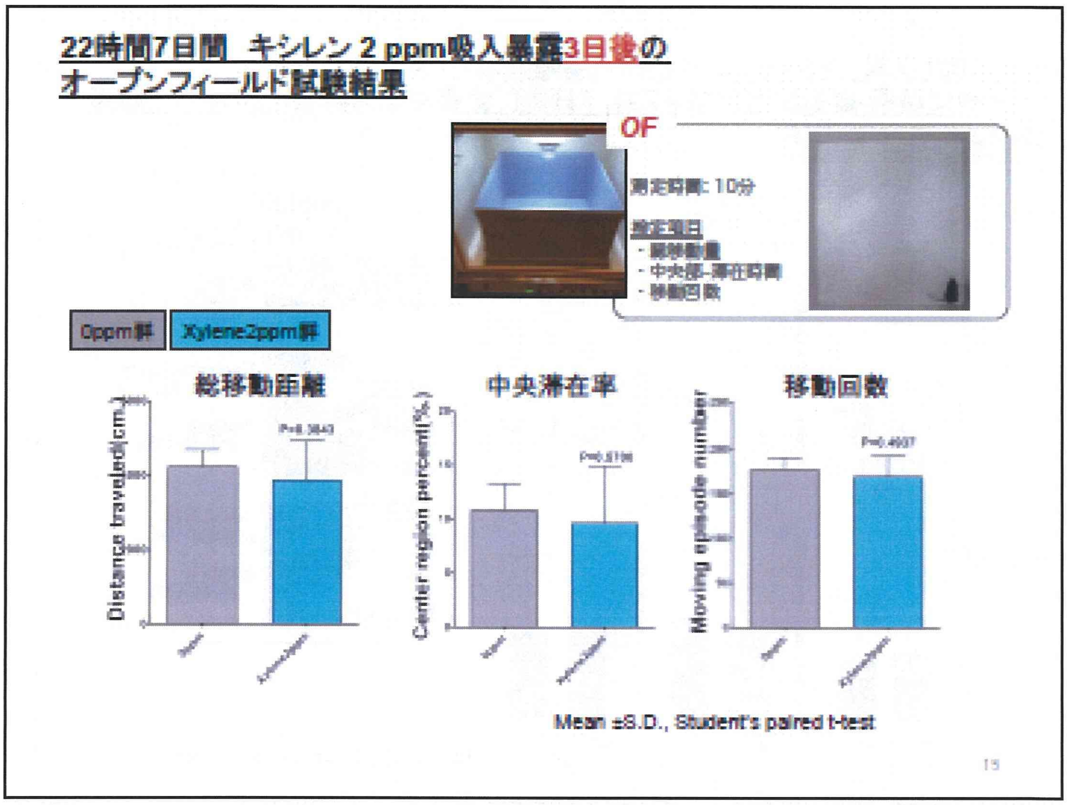
22時間7日間　キシレン 2 ppm吸入暴露3日後の
オープンフィールド試験結果
OF
測定時間: 10分
測定項目
・総移動量
・中央部-滞在時間
・移動回数
0ppm群
Xylene2ppm群
総移動距離
Distance traveled(cm)
中央滞在率
Center region percent(%)
移動回数
Moving episode number
Mean ±S.D., Student's paired t-test
15

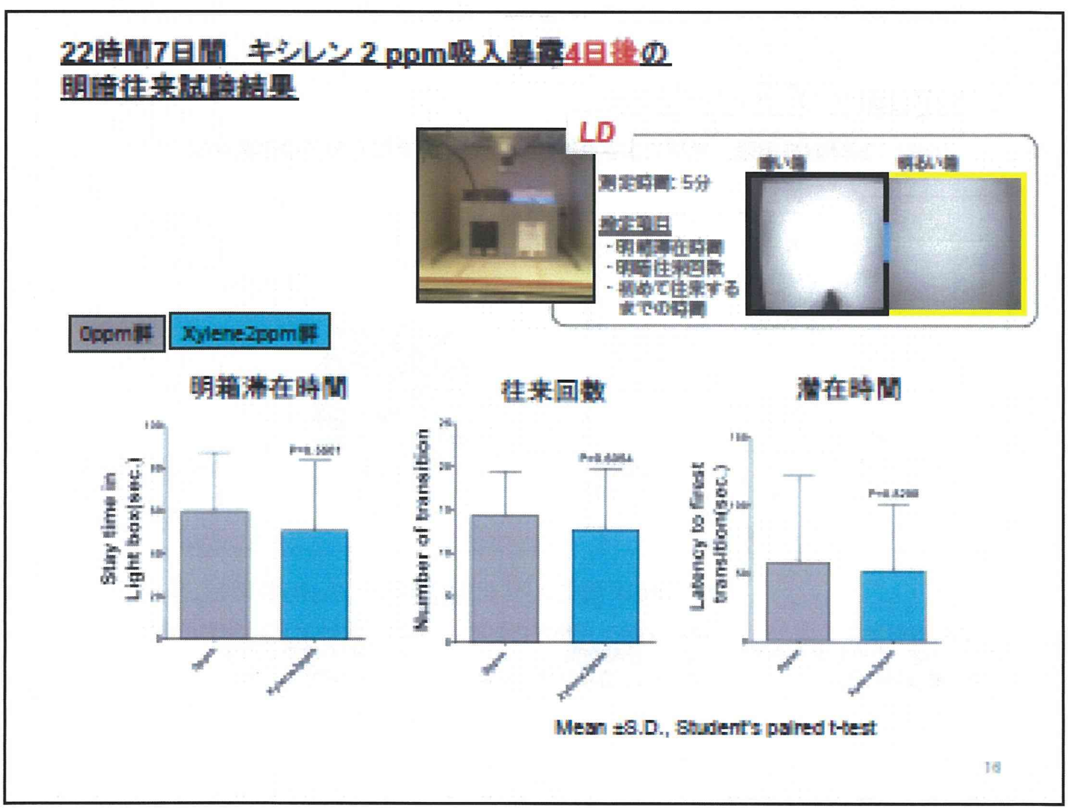
22時間7日間　キシレン 2 ppm吸入暴露4日後の
明暗往来試験結果
LD
測定時間: 5分
測定項目
・明箱滞在時間
・明暗往来回数
・初めて往来する
までの時間
0ppm群
Xylene2ppm群
明箱滞在時間
Stay time in
Light box(sec.)
往来回数
Number of transition
潜在時間
Latency to first
transition(sec.)
Mean ±S.D., Student's paired t-test
16

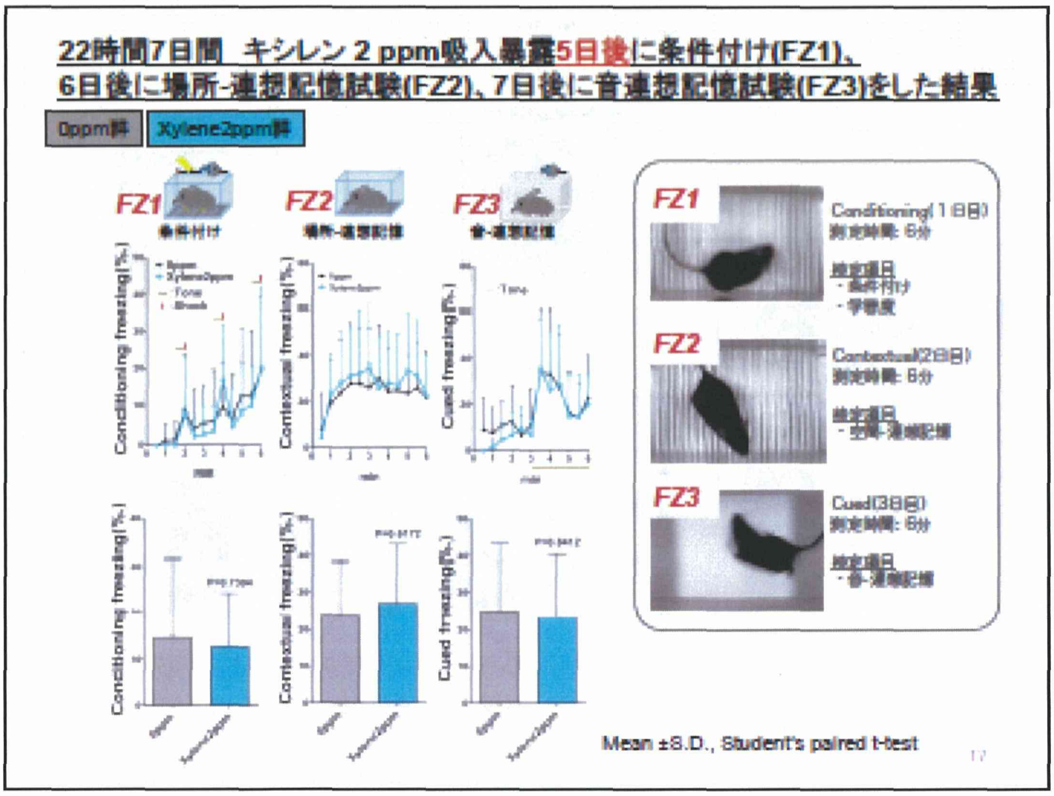

22時間7日間 キシレン 2 ppm吸入暴露5日後に条件付け(FZ1)、
6日後に場所-連想記憶試験(FZ2)、7日後に音連想記憶試験(FZ3)をした結果
0ppm群
Xylene2ppm群
FZ1
条件付け
FZ2
場所-連想記憶
FZ3
音-連想記憶
Conditioning freezing(%)
Contextual freezing(%)
Cued freezing(%)
FZ1
Conditioning(1日目)
測定時間: 6分
測定項目
・条件付け
・学習度
FZ2
Contextual(2日目)
測定時間: 6分
測定項目
・場所-連想記憶
FZ3
Cued(3日目)
測定時間: 6分
測定項目
・音-連想記憶
Mean ±S.D., Student's paired t-test
17

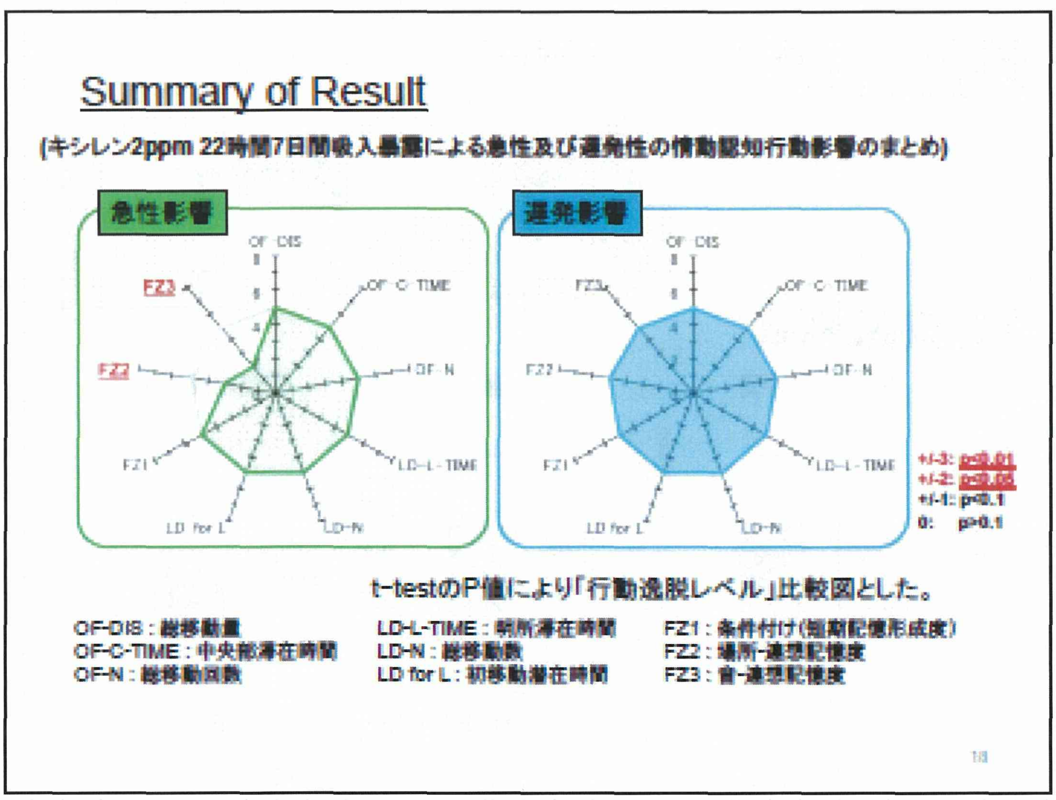

Summary of Result
(キシレン2ppm 22時間7日間吸入暴露による急性及び遅発性の情動認知行動影響のまとめ)
急性影響
遅発影響
OF-DIS
OF-C-TIME
OF-N
LD-L-TIME
LD-N
LD for L
FZ1
FZ2
FZ3
+/-3: p<0.01
+/-2: p<0.05
+/-1: p<0.1
0: p>0.1
t-testのP値により「行動逸脱レベル」比較図とした。
OF-DIS：総移動量
OF-C-TIME：中央部滞在時間
OF-N：総移動回数
LD-L-TIME：明所滞在時間
LD-N：総移動数
LD for L：初移動潜在時間
FZ1：条件付け(短期記憶形成度)
FZ2：場所-連想記憶度
FZ3：音-連想記憶度
18

結果

移動式行動解析装置によるマウス行動解析は、従来の結果を再現可能であり、本研究遂行に支障がないことが確認された。

吸入暴露後の行動影響解析の結果、暴露終了日の時点(急性影響の検討)では、オープンフィールド試験、明暗往来試験では対照群と比較し有意な変化は認められなかったが、条件付け学習記憶試験において空間-連想記憶及び音-連想記憶の有意な低下が認められた。一方、暴露3日後での解析では(遅発性影響の検討)、全ての試験項目で対照群と有意な差は認められなかった。

19

結論

吸入暴露による急性～亜急性の記憶異常を明確に捉えることに成功した。これは、SHSによる脳高次機能への影響を行動学的に捉えたものであり、今後、対応する神経科学的物証によって補強できると考えられる。

今回、捉えた成熟期の吸入暴露によって誘発される記憶異常は可逆的なものであったが、今後、幼若期におけるSHS相当の暴露影響については、遅発影響の有無を検討する必要がある。

20

別添５

Ⅲ．研究成果の刊行に関する一覧表

研究成果の刊行に関する一覧表

雑誌

発表者氏名	論文タイトル名	発表誌名	巻名	ページ	出版年
Tanaka M, Yamazaki Y, Kanno Y, Igarashi K, Aisaki K, Kanno J and Nakamura T	Ewing's sarcoma precursors are highly enriched in embryonic osteochondrogenic progenitors.	J Clin Invest	124 (7)	3061 - 3074	2014
Janesick A, Nguyen TT, Aisaki K, Igarashi K, Kitajima S, Chandraratna RA, Kanno J and Blumberg B	Active Repression by RARγ Signaling is Required for Vertebrate Axial Elongation.	Development	141 (11)	2260 - 2270	2014
Tanaka M, Aisaki K, Kitajima S, Igarashi K, Kanno J and Nakamura T	Gene expression response to EWS–FLI1 in mouse embryonic cartilage.	Genomics Data	2	296 - 298	2014
Hang NTL, Matsushita I, Shimbo T, Hong LT, Tam DB, Lien LT, Thuong PH, Cuong VC, Hijikata M, Kobayashi N, Sakurada S, Higuchi K, Harada N, Endo H and Keicho N	Association between tuberculosis recurrence and interferon-gamma response during treatment.	J Infect	69	616 - 626	2014
Shirakata Y, Hiradate Y, Inoue H, Sato E and Tanemura K	Histone h4 modification during mouse spermatogenesis.	J Reprod Dev	60 (5)	383 - 387	2014
Inoue H, Hiradate Y, Shirakata Y, Kanai K, Kosaka K, Gotoh A, Fukuda Y, Nakai Y, Uchida T, Sato E and Tanemura K	Site-specific phosphorylation of Tau protein is associated with deacetylation of microtubules in mouse spermatogenic cells	FEBS Lett	588 (11)	2003 - 2008	2014

別添 6

Ⅳ. 研究成果の刊行物・別刷

Research article

Ewing's sarcoma precursors are highly enriched in embryonic osteochondrogenic progenitors

Miwa Tanaka,[1] Yukari Yamazaki,[1] Yohei Kanno,[1] Katsuhide Igarashi,[2] Ken-ichi Aisaki,[2] Jun Kanno,[2] and Takuro Nakamura[1]

[1]Division of Carcinogenesis, The Cancer Institute, Japanese Foundation for Cancer Research, Tokyo, Japan.
[2]Division of Cellular and Molecular Toxicology, Biosafety Research Center, National Institute of Health Science, Tokyo, Japan.

Ewing's sarcoma is a highly malignant bone tumor found in children and adolescents, and the origin of this malignancy is not well understood. Here, we introduced a Ewing's sarcoma–associated genetic fusion of the genes encoding the RNA-binding protein EWS and the transcription factor ETS (*EWS-ETS*) into a fraction of cells enriched for osteochondrogenic progenitors derived from the embryonic superficial zone (eSZ) of long bones collected from late gestational murine embryos. *EWS-ETS* fusions efficiently induced Ewing's sarcoma–like small round cell sarcoma formation by these cells. Analysis of the eSZ revealed a fraction of a precursor cells that express growth/differentiation factor 5 (*Gdf5*), the transcription factor *Erg*, and parathyroid hormone-like hormone (*Pthlh*), and selection of the *Pthlh*-positive fraction alone further enhanced *EWS-ETS*–dependent tumor induction. Genes downstream of the EWS-ETS fusion protein were quite transcriptionally active in eSZ cells, especially in regions in which the chromatin structure of the ETS-responsive locus was open. Inhibition of β-catenin, poly (ADP-ribose) polymerase 1 (PARP1), or enhancer of zeste homolog 2 (EZH2) suppressed cell growth in a murine model of Ewing's sarcoma, suggesting the utility of the current system as a preclinical model. These results indicate that eSZ cells are highly enriched in precursors to Ewing's sarcoma and provide clues to the histogenesis of Ewing's sarcoma in bone.

Introduction

Ewing's sarcoma is a highly malignant bone tumor in children and adolescents. It frequently develops as a small round cell sarcoma in the metaphysis of long bones (1). The origin of Ewing's sarcoma has been an enigma since the first case was reported in 1921 (2). Primitive neural crest cells, hematopoietic cells, and muscle cells as well as mesenchymal stem cells (MSCs) have been considered possible cells of origin (3, 4). Chromosomal translocation-related genetic fusions between *EWSR1* on chromosome 22 and genes encoding ETS family transcription factors, such as *FLI1* and *ERG*, were then identified. The EWS and the transcription factor ETS (*EWS-ETS*) fusion is now considered a genetic hallmark of human Ewing's sarcoma (5–7). However, it has been difficult to establish an appropriate animal model by introduction of *EWS-ETS* chimeras (8), suggesting that introduction of *EWS-ETS* is not sufficient to define the origin of the tumors. A few groups have reported successful development of Ewing's sarcoma-like tumors by introduction of *EWS-FLI1* into murine mesenchymal cells (9, 10). However, it is unclear whether there is a special subfraction that includes the cell of origin of Ewing's sarcoma. The difficulty of inducing Ewing's sarcoma suggests that the target cells of *EWS-ETS* might be the cells of a narrow lineage and/or of a limited differentiation stage.

Unlike osteosarcoma, which generally involves the metaphyses of long tubular bones, Ewing's sarcoma occurs at almost equal frequencies in flat bones and the diaphysis of tubular bones (11). This fact suggests that mutations related to the proliferation of bony tissue might not contribute to the genesis of Ewing's sarcoma. Moreover, it suggests that the primary genetic event, the EWS-ETS fusion, might occur at an earlier stage of bone development.

Members of the *ETS* family of genes that are involved in *EWS* fusions are important for transcriptional regulation in mouse embryonic and perinatal limb skeletogenesis (12). Accumulation of *Erg*⁺ progenitor cells occurs in the embryonic superficial zone (eSZ) of long bones from dpc 15.5 to P7, after which expression is downregulated rapidly (13, 14). These results suggest that temporospatial expression of *Erg* might be critical for induction of bipotential progenitors during osteochondrogenic differentiation and that dysregulated expression due to chromosomal translocation and fusion to *EWSR1* might result in abnormal accumulation of progenitor cells that exhibit increased proliferative potency (10).

To clarify the possible cellular origin of Ewing's sarcoma, we purified eSZ cells from murine embryonic long bones that expressed *Erg* and introduced *EWS-FLI1* or *EWS-ERG* fusion genes. We found that EWS-ETS target cells were highly enriched in the eSZ fraction. Moreover, the epigenetic status of genes responsive to transcriptional regulation by EWS-ETS is important for Ewing's sarcoma development and its phenotypic manifestation.

Results

Development of Ewing's sarcoma–like small round cell tumors by EWS-ETS expression in the eSZ cells. *Erg*, one of the *EWS* fusion partners in Ewing's sarcoma, is transiently expressed in the joint surface of embryonic and perinatal bones. Therefore, we predicted that the *EWS-ETS* fusion would affect differentiation and induce abnormal proliferation of *Erg*-expressing cells. To test this hypothesis, femoral and humeral bones of dpc 18.5 murine embryos were separated into the eSZ, embryonic growth plate (eGP), the embryonic shaft and synovial regions (eSyR) by microdissection (Figure 1A). Embryonic mesenchymal cells of the head and trunk were also prepared. Each cell fraction was mildly digested with type I collagenase. The cells were immediately subjected to retrovirus-mediated

Conflict of interest: The authors have declared that no conflict of interest exists.
Citation for this article: *J Clin Invest*. 2014;124(7):3061–3074. doi:10.1172/JCI72399.

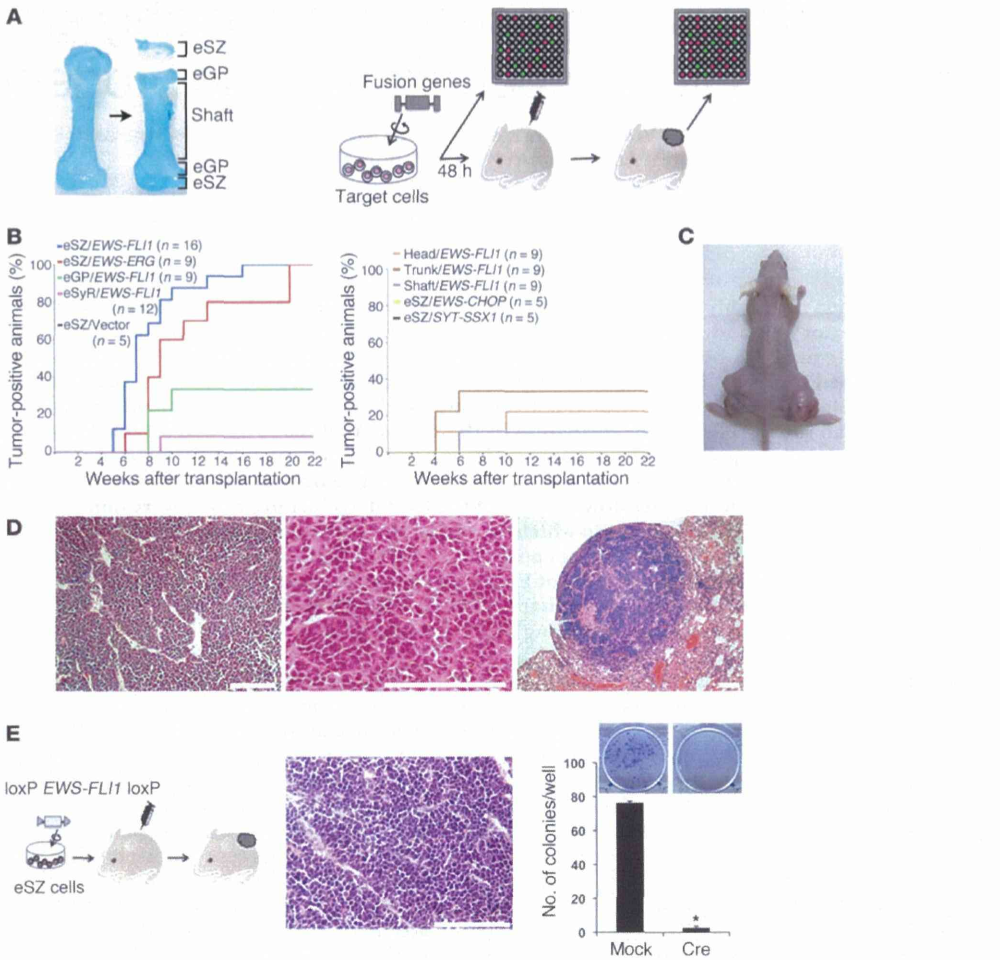

Figure 1

Development of murine Ewing's sarcoma. (**A**) Microdissection of mouse embryonic bone. The femur was lightly stained with methylene blue. Experimental strategy of the ex vivo model. Each cell type targeted with *EWS-ETS* was injected into nude mice or subjected to gene expression profiling. (**B**) Cumulative incidence (percentage) of small round cell tumors induced by eSZ, eGP, and eSyR cells expressing *EWS-ETS* or by eSZ with an empty vector and by embryonic mesenchymal cells of the trunk, head, and shaft expressing *EWS-FLI1* or eSZ expressing *EWS-CHOP* or *SYT-SSX1*. $P < 0.02$ in eSZ/*EWS-FLI1* vs. eGP, eSyR, or shaft; $P < 0.04$ in eSZ/*EWS-FLI1* vs. trunk and head, log-rank test. (**C**) Tumors were observed as subcutaneous masses in recipient nude mice. (**D**) Histology of murine Ewing's sarcoma. H&E staining, with low (left) and high (center) magnification. Pulmonary metastasis of murine Ewing's sarcoma developed by tail vein injection of tumor cells (right). Scale bar: 100 μm. (**E**) *Cre/loxP-mediated knockout of the EWS-FLI1 transgene. Ewing's sarcoma developed by transplantation of eSZ cells transduced with the* floxed *EWS-FLI1* retrovirus (left). Sarcoma cells were then maintained in vitro and transduced with the pMSCV-Cre retrovirus. Cre expression suppressed colony formation (right). The experiment was repeated 3 times and the representative results, are shown (graph inset). Scale bar: 100 μm. *$P < 0.01$. The mean ± SEM of 3 independent experiments is shown.

gene transfer of *EWS-FLI1* to all cell types by spin infection. The transduction efficiency was examined by flow cytometric analyses (Supplemental Figure 1A; supplemental material available online with this article; doi:10.1172/JCI72399DS1), and the expression of EWS-FLI1 was confirmed by FACS and immunofluorescent staining using anti-FLAG (Supplemental Figure 1, B–D). One million transduced cells of each fraction were injected subcutaneously into nude mice. Recipients transplanted with eSZ cells transduced with *EWS-FLI1* or *EWS-ERG* developed a subcutaneous mass at 100% penetrance, with a mean latency of 8 weeks (Figure 1, B–D).

As few as 1×10^4 injected transduced eSZ cells could develop Ewing's sarcomas. In contrast, 1×10^6 cells from *EWS-FLI1*-transduced eGP, embryonic shaft, or eSyR fractions were required for tumor development, clearly indicating that Ewing's sarcoma precursors were highly enriched in the eSZ fraction (Table 1). When embryonic mesenchymal cells purified from the mouse

Table 1
Summary of the incidences of tumors in limiting dilution experiments using eSyR, eSZ, eGP, shaft, trunk, or head cells

Cells	Numbers of transplanted cells		
	1×10^6	1×10^5	1×10^4
eSZ	25/25 (100%)	12/13 (92%)	4/5 (80%)
eGP	3/9 (33%)	0/7 (0%)	ND
eSyR	2/12 (17%)	0/10 (0%)	ND
Shaft	1/9 (11%)	0/6 (0%)	ND
Trunk	3/9 (33%)	1/10 (10%)	0/5 (0%)
Head	2/9 (22%)	1/7 (14%)	0/5 (0%)

ND, not done.

head or trunk were transduced with *EWS-FLI1*, the incidence of small round cell sarcomas was again lower, and fibrosarcoma-like tumors were also obtained (Figure 1B and Supplemental Figure 2A). In addition, no tumor was induced when *EWS-CHOP* or *SYT-SSX1*, which are found in myxoid liposarcoma or synovial sarcoma, respectively, were introduced into eSZ cells (Figure 1B). Development of nonneoplastic bone and cartilage was observed when we transplanted eSZ cells treated with an empty vector (Supplemental Figure 2B).

Histological analysis showed that tumors expressing *EWS-FLI1* or *EWS-ERG* were composed of aggressively growing, small round cells, a feature typical of Ewing's sarcoma (Figure 1D). All the tumors examined (10 of 10) were capable of secondary transplantation (Supplemental Table 1 and Supplemental Figure 2C), and 3 of 9 tumors had metastatic potential by tail vein injection (Figure 1D, Supplemental Table 1, and Supplemental Figure 2D). EWS-ETS expression was confirmed by immunoblotting and immunostaining of FLAG-tagged proteins (Supplemental Figure 2E). MIC2 (also known as CD99), a surface marker for human Ewing's sarcoma (15), was focally detected (Supplemental Figure 2F). *Cd99* gene sequences are only partially conserved between human and mouse (16), and therefore, CD99 was not useful as a specific marker for murine Ewing's sarcoma.

Cre/loxP-mediated genetic recombination and knockout of the *EWS-FLI1* transgene induced complete growth arrest of the tumor (Figure 1E), and senescence-like cellular phenotypes were observed in 91.4% of surviving cells (1.4% in non-Cre-treated cells) (Supplemental Figure 3). Thus, murine Ewing's sarcoma is dependent on *EWS-FLI1* activity. These results indicate that cellular targeting of eSZ cells by *EWS-ETS* fusion genes efficiently and specifically induced human Ewing's-like sarcoma in mice.

In addition, the monoclonal or oligoclonal nature of murine Ewing's sarcoma was indicated by cloning of retroviral integration sites (Supplemental Excel File 1). The tumors (n = 21) contained an average of 2.5 integration sites, and no common integration site has been identified, although there are interesting genes involved in neoplastic processes, such as *Ccnd3*, *Junb*, *Bach2*, and *Fyn*.

eSZ cells were characterized as osteochondrogenic progenitors. After condensation of mesenchymal stem/progenitor cells, the primitive structure of joint surfaces develops, and a chondrogenic progenitor lineage-rich eSZ emerges on the joint surface to develop the long bone from dpc 15.5 to P7 (Figure 2A and refs. 13, 17). eSZ cells purified by microdissection were positive for CD29 but lacked surface markers for MSC, such as SCA1, CD34, CD44, and CD105, in contrast to embryonic trunk cells (Supplemental Figure 4A). eSZ cells were also negative for Gr-1, FLK1, and CD45 (Supplemental Figure 4A and data not shown). These data indicated that eSZ cells constituted a different cohort from those making up the previously defined MPC fraction that is positive for CD44, Thy1 (CD90), and SCA1 (9).

We compared gene expression profiles of purified eSZ and eGP cells obtained by microdissection. The results suggested that eSZ cells were an immature chondrogenic precursor (Supplemental Table 2 and Supplemental Excel File 2). Furthermore, laser microdissection, followed by expression analyses of a series of differentiation-related genes, was carried out to assess the gene expression profile of the eSZ fraction (Figure 2, B–D). As expected, *Erg* and growth/differentiation factor 5 (*Gdf5*) expression was prominent in eSZ cells. Moreover, eSZ cells showed gene expression profiles characteristic of immature chondrogenic precursors, including parathyroid hormone-like hormone (*Pthlh*), *Prg4*, and *Col2a1*, consistent with previous studies (Figure 2C and refs. 12, 18, 19). On the other hand, eGP cells showed a more differentiated chondrocytic gene expression profile, as represented by *Col10a1* (Figure 2C). Also, *Nanog*, *Oct4*, and *Sox2* (together denoted as NOS), which are expressed in most immature lineages, were enriched in eSyR, whereas little or no expression was observed in eSZ or eGP fractions. The results are summarized in Table 2, and they indicate that enrichment of an $ERG^{hi}/GDF5^{hi}/PTHLH^{hi}/PRG4^{hi}/NOS^{lo}$ fraction was achieved by fine selection of eSZ cells. *Gdf5* was transiently expressed in eSZ cells and is a master regulator of joint formation (20). *Gdf5* promoter activity was also exhibited exclusively in eSZ cells (Supplemental Figure 4B).

In an in vitro differentiation assay, eSZ cells exhibited remarkable osteogenic and chondrogenic differentiation potencies but lacked the ability to differentiate into the adipogenic lineage. In contrast, embryonic mesenchymal progenitor cells showed their typical multilineage differentiation pattern (Figure 2D). Adipogenesis-related genes, such as *Pparg* and *Fabp4*, were not expressed in eSZ cells, but they were observed in eSyR cells (Supplemental Figure 4C). Also, eSZ cells were unable to differentiate into myogenic or neuronal lineages (Supplemental Figure 4D).

The tumor induction efficiency was further enhanced by immune selection of the eSZ cells using PTHLH (Supplemental Figure 1D), a marker that is expressed by periarticular cells and articular chondrocytes (17, 21, 22). All the recipients transplanted with 1×10^4 $PTHLH^+$ eSZ cells developed Ewing's sarcoma with a significantly shorter latency than that of those receiving unselected eSZ cells ($P < 0.01$). In contrast, no tumors were developed by recipients of the $PTHLH^-$ fraction of eSZ cells (Figure 2E; see complete unedited blots in the supplemental material). In addition, $PTHLH^+$ eSZ cells showed higher expression of *Erg* and *Gdf5* than the $PTHLH^-$ fraction (Figure 2F). These findings indicated that bipotential progenitors were present in the eSZ fraction and that successful enrichment of Erg^+ and $Pthlh^+$ progenitor cells was achieved in the eSZ cell fraction. eSZ cells were therefore used for the *EWS-ETS* gene transfer and subsequent transplantation experiments.

Early neoplastic lesions of murine Ewing's sarcoma. Our new animal model enabled us to examine how malignant cells progressed from preneoplastic and/or early neoplastic stages of cancer, stages that are difficult to observe in human Ewing's sarcoma (23). Early lesions of murine Ewing's sarcoma were therefore analyzed microscopically (Figure 3). Small foci of EWS-FLI1–positive (FLAG-positive) cells were observed adjacent to nonneoplastic cartilage (Figure 3A). Rapid cell cycle progression was confirmed in assess-

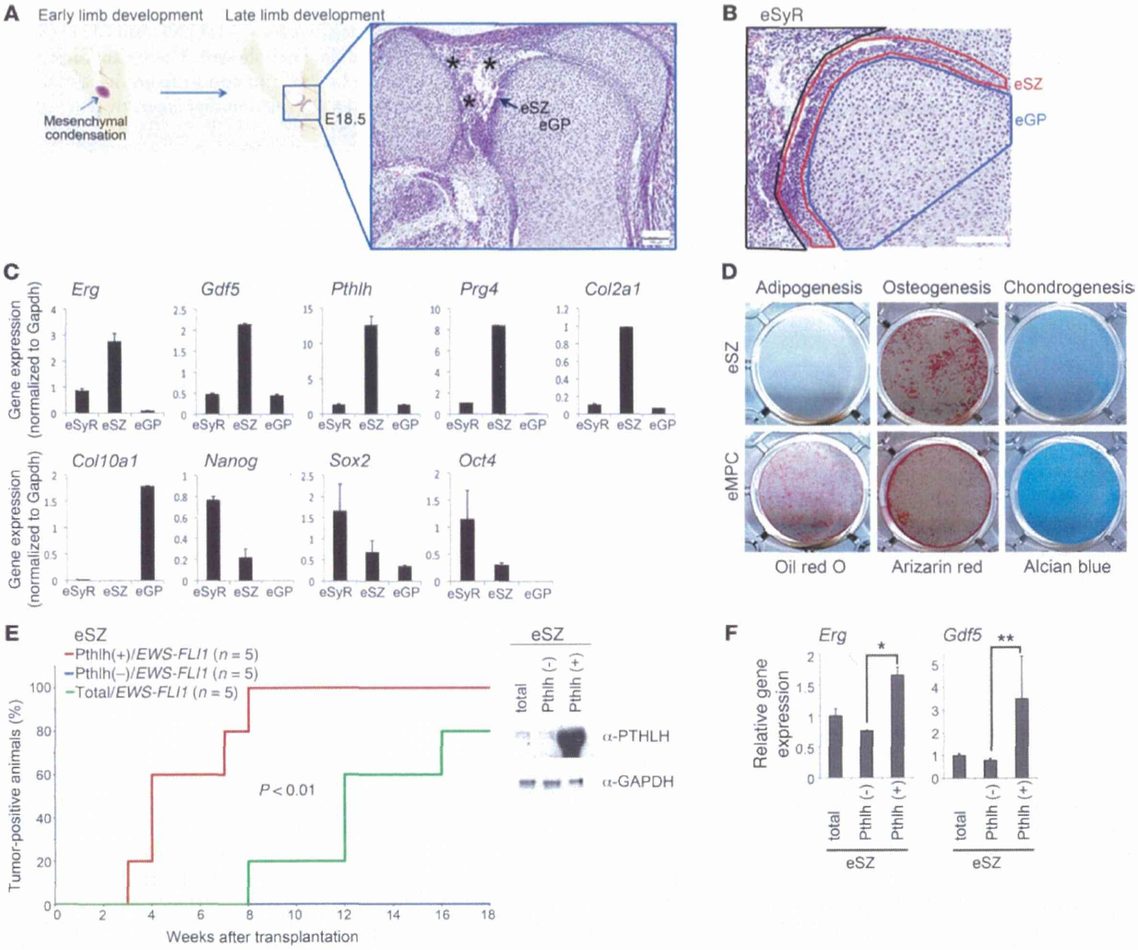

Figure 2

Characterization of eSZ cells. (**A**) Schematic illustration and histology of the developing knee joint in dpc 18.5 embryo. eSZ and eGP are indicated. Asterisks denote eSyR. Scale bar: 100 μm. (**B**) eSZ, eGP, and eSyR components were fractionated by laser microdissection and subjected to gene expression analysis. Scale bar: 100 μm. (**C**) Differentially expressed genes among eSyR, eSZ, and eGP cells. Quantitative RT-PCR analysis for *Erg*, *Gdf5*, *Pthlh*, *Prg4*, *Col2a1*, *Col10a1*, *Nanog*, *Sox2*, and *Oct4* expression in eSyR, eSZ, and eGP cells. The mean ± SEM of 3 independent experiments are shown. (**D**) In vitro differentiation assays of eSZ cells and trunk mesenchymal progenitor cells (eMPC). Adipogenic, osteogenic, and chondrogenic differentiation was induced in embryonic mesenchymal progenitor cells, whereas eSZ cells showed no adipogenic differentiation. The experiment was repeated 3 times, and representative results are shown. (**E**) PTHLH$^+$ and PTHLH$^-$ fractions were separated using biotinylated anti-PTHLH and avidin-conjugated magnetic beads. Tumor induction was examined by transplantation of each fraction (1×10^4 cells). $P < 0.01$ in PTHLH$^+$ eSZ/*EWS-FLI1* vs. total eSZ, log-rank test. Condensation of the PTHLH$^+$ fraction was confirmed by immunoblotting. (**F**) Expression of *Erg* and *Gdf5* in PTHLH$^+$ and PTHLH$^-$ eSZ cells. The mean ± SEM of 3 independent experiments are shown. $^*P < 0.01$; $^{**}P < 0.05$.

ments of BrdU incorporation (Figure 3B). The early neoplastic lesions did not express neural, myogenic, epithelial, vascular, or hematopoietic markers, including CD57, NGFR, S-100, myosin, desmin, von Willebrand factor, cytokeratin, or CD45 (data not shown). A few FLAG-positive cells expressed collagen type 2, a marker of immature chondrocytes (18, 24), and were observed in the peripheral areas around the early neoplastic foci (Figure 3C). Interestingly, these differentiating cells exhibited cytoplasmic staining for EWS-FLI1. Staining was essentially localized to the nucleus in the central part of the early neoplastic lesion (Figure 3B). Whereas nuclear localization of EWS-FLI1 fusion protein has been confirmed in most cell types (25), its cytoplasmic localization in differentiating cells suggests that cytoplasmic exclusion of EWS-FLI1 might represent an inhibitory mechanism in tumorigenesis of Ewing's sarcoma. The existence of cytoplasmic exclusion suggests that EWS-FLI1 expression alone is insufficient to induce complete tumorigenesis. In addition, more differentiated chondrocytes, positive for S100 or collagen type 10, were observed

Table 2
Summary of eSZ cell profiles

Gene	Expression properties	
	Levels in eSZ	Other mesenchymes
Erg	High	SZ (E)
Gdf5	High	SZ (E)
Pthlh	High	SZ (E, A)
Prg4	High	SZ (E, A)
Col2a1	Moderate	Proliferating chondrocytes (E, A)
Col10a1	None	Hypertrophic chondrocytes (E, A)
Nanog	Low	ES, EMPC
Sox2	low	ES, EMPC
Oct4	low	ES, EMPC

SZ, superficial zone or articular cartilage; ES, embryonic stem cell; EMPC, embryonic mesenchymal progenitor cell. Parenthetical E or A indicate embryo or adult, respectively.

in the surrounding area (Figure 3D and Supplemental Figure 5). EWS-FLI1 expression was hardly detected in S100-positive cells (Figure 3D). Microdissection and gene expression analyses of early neoplastic lesions revealed continued expression of *Erg*, *Gdf5*, *Pthlh*, and *Prg4*, whereas, in differentiated areas, downregulation of those genes was accompanied by increased *Col10a1* expression (Figure 3E). Those results indicated that the nature of the eSZ is preserved in the early neoplastic lesion, at least in part.

Murine Ewing's sarcoma shared common gene expression profiles with human small round cell tumor, including Ewing's sarcoma and neuroblastoma. Expression profiles of murine Ewing's sarcomas were compared with those of a series of human sarcomas, including Ewing's sarcoma, malignant fibrous histiocytoma, myxoid liposarcoma, synovial sarcoma, osteosarcoma, neuroblastoma, and chondrosarcoma. Hierarchical clustering using common gene sets between mice and humans (1,819 probes selected from 23,860 probe sets) showed that the murine Ewing's sarcoma was quite similar to the human Ewing's sarcoma and neuroblastoma (Figure 4A). The results suggested a relationship between the present model and human Ewing's sarcoma. Moreover, the neuroblastoma-like small round cell morphology could be induced from osteochondrogenic precursor cells by *EWS-FLI1* expression.

To better understand the nature of the small round tumor cells, the expression profile of mouse Ewing's sarcoma was again compared with that of human Ewing's sarcoma, poorly differentiated synovial sarcoma, neuroblastoma, and malignant lymphoma, and the profile of human Ewing's sarcoma was compared with that of mouse tumors (Figure 4B). Two thousands probe sets "specific" for each tumor that showed larger differences of expression relative to the rest of the tumor types were selected in both human and mouse tumor groups. Then, lists of the 2,000 probes were compared between mouse Ewing's sarcoma and each human tumor and between human Ewing's sarcoma and each mouse tumor, resulting in the selection of human and mouse Ewing's sarcoma as the closest counterparts to each another (Figure 4B), though the data were not statistically significant except for malignant lymphoma. Collectively, these data indicate that the expression profiles depend in part on the cell morphology of the small round cell tumor. It is notable that EWS-FLI1 expression in murine eSZ cells could induce human Ewing's sarcoma-like gene expression profiles.

Common upregulated genes in murine and human Ewing's sarcoma are presented in Supplemental Excel File 3 and Supplemental Figure 6A. The analysis revealed that 336 genes were upregulated in both murine and human Ewing's sarcomas, including known EWS-FLI1 targets such as *Dkk2*, *Prkcb1*, enhancer of zeste homolog 2 (*Ezh2*), *Id2*, *Nkx2.2*, *Nr0b1*, and *Ptpn13* (26–32). Furthermore, 6,014 genes, including EWS-FLI1 targets such as *Aurka*, *Gstm4*, *Tert*, *Tnc*, and *Upp1*, were upregulated in murine Ewing's sarcoma (Figure 4C, Supplemental Excel File 3, and refs. 33–37). These 5 genes were identified by EWS-FLI1 overexpression or silencing studies or by an immunohistochemical analysis that might cause exclusion of them as upregulated genes in human Ewing's sarcoma. Twenty-two out of thirty upregulated targets proposed by Ordonez et al. (8) were indeed upregulated in our model. In addition, 360 genes (including *Tgfbr2*) (38) were downregulated in both murine and human Ewing's sarcoma (Supplemental Figure 6A and Supplemental Excel File 4). These genes were potentially EWS-FLI1-responsive genes and might be important in the early oncogenic process as well as in the progression toward more malignant phenotypes. These gene expression results support the authenticity of our murine model for human Ewing's sarcoma.

The same analysis showed that 129 genes were upregulated in both murine and human Ewing's sarcoma as well as human neuroblastoma. Upregulation of a series of neuronal differentiation-related genes (*Gfra2*, *Ncan*, *Nrxn1*, and *Ntrk1*) and synapse-related genes (Supplemental Figure 6B) in murine Ewing's sarcoma was also observed in human neuroblastoma, indicating that the neuronal phenotype could be induced from osteochondrogenic progenitors, probably through transdifferentiation processes. The neuroectodermal-related signaling pathway, including NTRK1/NTRK3 and N-MYC, might play some role in neuronal phenotypes of Ewing's sarcoma. Although the number of commonly upregulated genes in murine Ewing's sarcoma and neuroblastoma was larger than that in murine and human Ewing's sarcoma, most of the known target genes described above were included in the latter category, suggesting that the core mechanisms of EWS-FLI1 transcriptional regulation might be preserved in our model.

EWS-FLI1–responsive genes and chromatin modification in eSZ cells. The relationship between the cell of origin of Ewing's sarcoma and *EWS-ETS* fusions is important, given the strict limitations on the origin of murine Ewing's sarcoma. Gene expression profiles were therefore compared between eSZ and eGP cells in the presence or absence of *EWS-FLI1* (Figure 5A and Supplemental Excel File 5) (data are available at NCBI Gene Expression Omnibus [GEO] with accession number GSE32618). Most of the known EWS-FLI1 target genes (8) were upregulated in eSZ cells following *EWS-FLI1* introduction (Supplemental Excel File 5). *EWS-FLI1* encodes an aberrant transcription factor (8, 30), and the response to it differed between eSZ and eGP cells (Figure 5B, Supplemental Figure 7, and Supplemental Excel File 6). The different gene responses in eSZ and eGP cell fractions were probably caused by differences in chromatin conditions at target loci. Histone modifications were therefore examined on representative genes, such as *Dkk2*, *Prkcb1*, and *Ezh2*. Histones H3K9/K14ac and H3K4me, which are activation marks for gene expression, were observed predominantly in eSZ cells as well as mouse Ewing's sarcoma cells, whereas histone H3K9me3 and H3K27me3, which are repressive marks, were observed predominantly in eGP cells (Figure 5C). These results strongly suggest that transcriptional activation of EWS-ETS target genes occurred in eSZ cells at maximum efficiency and that

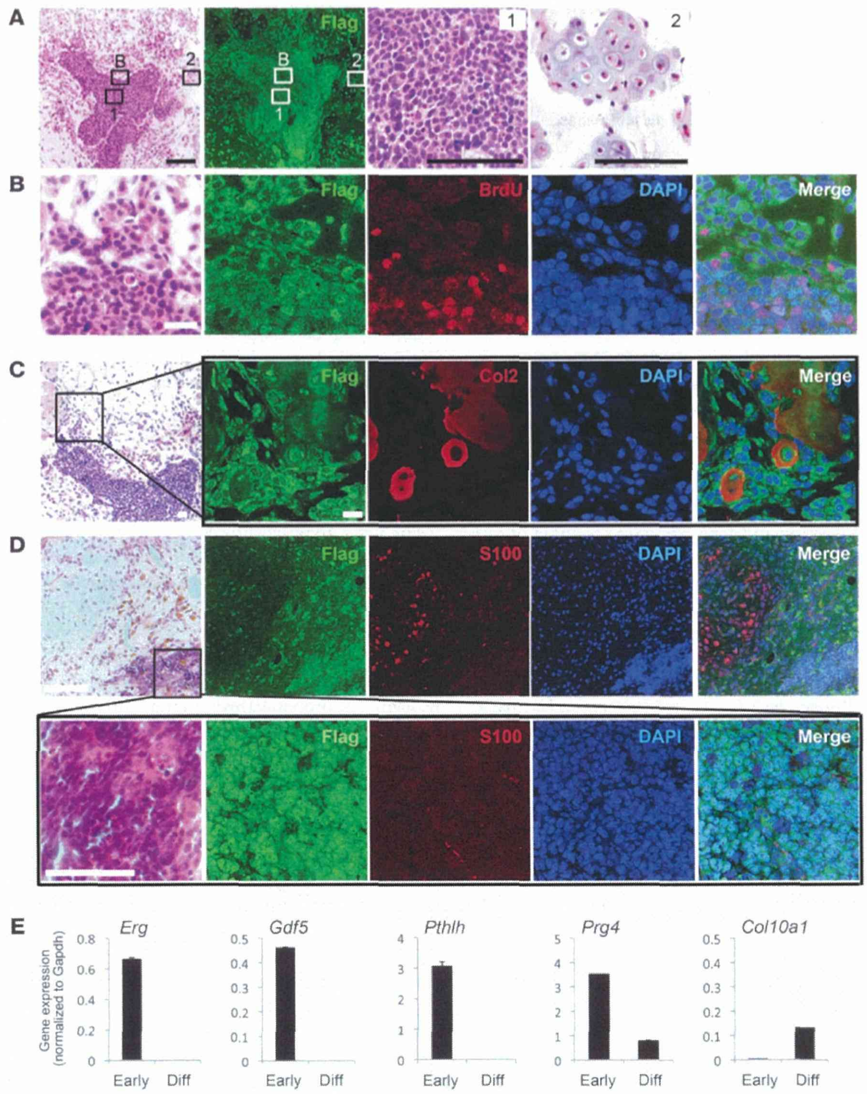

Figure 3

An early neoplastic lesion of murine Ewing's sarcoma 3 weeks after transplantation. (**A** and **B**) Immunofluorescent assessment of FLAG. (**A**) High-power images of early neoplastic cells (see boxed region 1 shown at higher magnification) and nonneoplastic cartilage (see boxed region 2 shown at higher magnification) are shown. Scale bar: 100 μm. (**B**) The boxed region in **A** shown at higher magnification. Accumulation of BrdU-positive nuclei in the central early neoplastic lesions. Nuclear localization of EWS-FLI1 (FLAG) was observed in the central region, whereas cytoplasmic translocation of EWS-FLI1 is remarkable in the differentiating zone. Scale bar: 20 μm. (**C**) The differentiating zone with cytoplasmic EWS-FLI1 staining is characterized by collagen 2 expression. Scale bar: 20 μm. (**D**) Further differentiation toward the chondrogenic lineage in a more peripheral area is indicated by expression of S100 (top row), which is negative in the central early neoplastic lesion (bottom row). Scale bar: 100 μm. (**E**) Quantitative real-time PCR analysis for *Erg*, *Gdf5*, *Pthlh*, *Prg4*, and *Col10a1* expression in early neoplastic cells and the differentiating zone. The mean ± SEM of 3 independent experiments are shown.

the histone status in eSZ cells was preserved after transformation, thereby providing the aggressive oncogenic function of EWS-ETS.

Upregulation of the WNT/β-catenin pathway in eSZ cells and in Ewing's sarcoma cells. Gene set enrichment analyses (GSEA) using gene sets of *EWS-FLI1*-expressing eSZ and eGP cells 48 hours after gene introduction exhibited enrichment of genes within the WNT/β-catenin pathway as well as the EGF and RTK signaling pathways (Figure 6A and Supplemental Figure 7). In the

WNT/β-catenin pathway, the expression of *Dkk2* and *Wif1* was observed in eSZ cells expressing *EWS-FLI1* (Figure 5B and Figure 6B). *Dkk2* expression was comparable between parental eSZ and eGP cells, and *EWS-FLI1* introduction induced upregulation of *Dkk2* only in eSZ cells (Figure 5B and Figure 6B). In contrast, expression of *Dkk1*, which is antagonistic to DKK2, remained unaltered by *EWS-FLI1* introduction in eSZ cells. Higher *Wif1* expression was observed in eSZ cells but not in eGP cells, and the difference in expression between eSZ and eGP cells was preserved after *EWS-FLI1* introduction. The WNT/β-catenin pathway was not enriched when gene sets of nontransduced eSZ and eGP cells were tested (data not shown). In addition, gene sets for the EGF pathway and receptor protein kinase activity were enriched (Figure 6B and Supplemental Figure 8). *Prkcb1* is a gene downstream from EWS-FLI1 (39) and is inherently expressed at higher levels in eSZ cells than in eGP cells. Notably, its expression was increased to higher levels by introducing *EWS-FLI1* into eSZ cells. *Flt4* (also known as *VEGFR3*) and *Musk*, which are important in signaling of vascular and neuromuscular systems, were also identified as EWS-FLI1-responsive genes (Figure 6B and Supplemental Figure 8). Furthermore, IGF1R and IGF2R, which are involved in IGF1 signaling and are attractive targets in Ewing's sarcoma therapy (40, 41), were also identified by GSEA (Supplemental Figure 8).

Dkk2 is a member of the dickkopf family of proteins. As modulators of the WNT/β-catenin pathway, this family plays important roles in the development and homeostasis of bone and cartilage (42). A previous study showed that *DKK2* was downregulated upon *EWS-FLI1* knockdown in Ewing's sarcoma cells, while the opposite response was observed in *DKK1* (26). Although previous studies suggested that DKK1 and DKK2 might have functions independent of the canonical WNT/β-catenin pathway (43), possible roles of WNT activation in human Ewing's sarcoma were reported (44).

To confirm the involvement of the WNT/β-catenin pathway in tumorigenesis of Ewing's sarcoma, expression of β-catenin protein was evaluated. β-Catenin expression was increased by transient introduction of *EWS-FLI1* into eSZ cells (Supplemental Figure 9A). As described above, murine Ewing's sarcoma was serially transplantable into syngeneic mice and showed high potency of proliferation (Supplemental Figure 2C). In the invasive area of the secondary tumor, increased expression of β-catenin was frequently observed (Supplemental Figure 9B). RNA interference-mediated *EWS-FLI1* knockdown resulted in decreased transcriptional activities of β-catenin (Supplemental Figure 9C). Collectively, these data indicate strong association between the upregulation of WNT/β-catenin signaling and cell growth of Ewing's sarcoma.

Inhibition of tumor growth by suppression of critical signals. The result indicates that EWS-FLI1 and its downstream signals are effective targets for therapy. Indeed, gene knockdown experiments showed that tumor cell proliferation was significantly inhibited by siRNA treatments specific for *Fli1*, *Dkk2*, *Catnb*, *Prkcb1*, *Ezh2*, or *Igf1* (Figure 6C). Knockdown of the same genes in the human Ewing's sarcoma cells showed similar suppression of cell proliferation (Supplemental Figure 10). Moreover, suppression of the EGF/RAS/MAPK pathway by a MEK1 inhibitor (U0126) showed inhibition of tumor growth in vitro in a dose-responsive manner (Figure 6D). These results demonstrated the importance of the signaling pathways activated by EWS-FLI1 in the progression of Ewing's sarcoma and its potential as a novel target for clinical treatment.

Use of the mouse model to test therapy targeted against Ewing's sarcoma. Animal models of human cancer provide platforms for evaluation of novel therapies. Ideally, the phenotypes and developmental mechanisms of the human and model systems should be similar. In this context, specific inhibitors of the WNT/β-catenin pathway, EZH2 and poly (ADP-ribose) polymerase 1 (PARP1), were tested using the current model both in vitro and in vivo. The β-catenin inhibitors, iCRT14 and PNU74654, showed marked growth suppression of both mouse and human Ewing's sarcoma, and an EZH2 inhibitor DZNeP showed modest but substantial growth suppression (Figure 7A and Table 3). Moreover, olaparib, a PARP1 inhibitor reported to exhibit Ewing's sarcoma-specific growth inhibition (45), also inhibited both mouse and human Ewing's sarcomas (Figure 7A and Table 3). Cell cycle analyses showed that iCRT14 and DZNeP induced cell cycle arrest, as indicated by increased G_1 populations and decreased G_2/M populations (Figure 7B). PNU74654 and olaparib also increased a sub-G_1 population, indicating apoptosis induction (Figure 7B). These reagents also suppressed in vivo growth of Ewing's sarcoma, with the greatest effect observed with iCRT14, followed by olaparib, DZNeP, and PNU74654 (Figure 7C). Thus, the current model provides an effective tool to explore and evaluate novel therapeutic drugs both in vitro and in vivo.

Discussion

Here, we demonstrate efficient and specific induction of a mouse equivalent of human Ewing's sarcoma. We showed that the origin of the tumor is closely related to embryonic osteochondrogenic progenitor cells. Selection of a PTHLH-expressing cellular fraction in eSZ enabled us to obtain substantially higher efficiency and greater specificity and consistency of tumor formation than previously reported investigations using bone marrow-derived mesenchymal stem/progenitor cells (9, 10). In addition, *EWS-FLI1* expression induced apoptosis and growth arrest in several cell types, including embryonic fibroblasts (46, 47). These data indicate that induction of Ewing's sarcoma by *EWS-ETS* fusion genes is much more effective for progenitor cells of a certain cell lineage, including the osteochondrogenic axis, especially in developing bone. A previous study indicated that *EWS-FLI1* induces cancer stem cell properties in pediatric MSCs but not in adult MSCs (48). The plasticity for cellular differentiation in embryonic and pediatric precursor cells might be important for Ewing's sarcoma development in younger patients. Moreover, EWS-ETS might induce the development of small round cells and neuroectoderm-like phenotypes.

Ewing's sarcoma is a rather rare neoplasm that affects children and adolescents with an incidence of 2.1 cases per million children (49). The low incidence of disease is also observed in other translocation-related sarcomas affecting young people, such as alveolar rhabdomyosarcoma, clear cell sarcoma, synovial sarcoma, or myxoid liposarcoma (50). This is in contrast to acute myeloid leukemia (AML), which is also characterized by gene fusion. It is likely that the difference in frequencies between sarcomas and AMLs is due to the rarity of progenitor cell populations in which chromatin conditions necessary for the oncogenic action of EWS-ETS are present. Such a narrow window of target cell emergence reflects the difficulty of inducing tumor in vivo models.

Once the EWS-FLI1 fusion occurs in an eSZ cell during the perinatal period or even in utero, the cell survives with acquired growth advantages. After a decade of incubation that allows additional genetic/epigenetic events in the mutated eSZ cell, Ewing's sarcoma eventually emerges in the bone as a highly aggressive tumor in human child-